Appl. Phys. A 81, 877–879 (2005)
DOI: 10.1007/s00339-004-2899-0

Applied Physics A
Materials Science & Processing

Y. CHANG[1]
Y.-K. KUO[2,✉]

A numerical study of dc characteristics of HEMT with *p*-type *δ*-doped barrier

[1] Department of Materials Science and Engineering, National Chiao Tung University, Hsinchu 30077, Taiwan
[2] Department of Physics, National Changhua University of Education, Changhua 50058, Taiwan

Received: 23 February 2004/Accepted: 19 April 2004
Published online: 30 June 2004 • **© Springer-Verlag 2004**

ABSTRACT The dc characteristics of an InGaP/InGaAs/GaAs pseudomorphic high-electron-mobility transistor (HEMT) with a *p*-type *δ*-doped InGaP barrier are numerically investigated with the ISE-TCAD simulation program. The simulation results indicate that a HEMT with such a structure has a higher gate turn-on voltage, better carrier confinement that results in a lower voltage-dependent transconductance, and a larger breakdown voltage when compared with the typical HEMT. The simulation results also suggest that this structure is beneficial for linear and large-signal application.

PACS 85.30.De; 73.50.-h; 02.60.Cb

1 Introduction

Over the past few years, heterostructure field-effect transistors (HFETs), heterostructure bipolar transistors (HBTs), and high-electron-mobility transistors (HEMTs) have been widely investigated for high-power and high-frequency integrated circuit applications. The InGaAs-based pseudomorphic HEMTs have received much attention due mainly to their application in high-speed transistors. However, the onset of parallel conductance in high-band-gap doping layers leads to a sharp peak in transconductance, which becomes a limitation for linear operation. In addition, due to the large need of high-power devices, enlarging the breakdown voltage is an important issue. Hence, much effort has been made by many research groups to increase the Schottky-barrier potential and to enhance the band offset between the channel and barrier layers.

From the literature [1–6] we note that it is beneficial to use InGaP, instead of AlGaAs, in the barrier layers. Firstly, InGaP has lower deep-level traps and lower DX centers and thermal oxidation when compared with AlGaAs. Hence, a higher stability can be obtained with InGaP. Secondly, the band gap of InGaP is larger than that of AlGaAs, which is beneficial for improving the breakdown voltage. Moreover, the relatively high etching selectivity between InGaP and GaAs makes it easy to control the process. In the meantime, p^+ doping in InGaP barrier layers can be used to further enlarge the barrier height [5–10], which in turn results in increased carrier confinement. Therefore, low leakage current, high breakdown voltage, and high linearity in transconductance can be expected.

It is believed that a HEMT with a *p*-type *δ*-doped InGaP barrier can have larger turn-on and breakdown voltages than a typical HEMT, because the *p*-type doping enlarges the barrier potential in the conduction band and the electric field produced by the negative charges in the depleted *p*-type region may prevent electron leakage under reverse gate bias. In this paper, the dc characteristics of a HEMT with a *p*-type *δ*-doped InGaP barrier are numerically investigated with the ISE (integrated system engineering)-TCAD (technology computer-aided design) simulation program. Specifically, the transconductances of the typical HEMT and HEMTs with *p*-type *δ*-doped barriers of various doping concentrations are investigated.

2 Structures of the HEMTs under study

The structures of a typical InGaP/InGaAs/GaAs pseudomorphic HEMT and a HEMT with a *p*-type *δ*-doped InGaP barrier are shown in Fig. 1a and b, respectively. The channel thickness of each device is 100 Å and the indium composition is 20%. The 50-Å-thick GaAs sub-spacer is used for diverting hot electrons back to the upper *n*-type *δ*-doped layer. Two 30-Å-thick AlGaAs spacers are located above and below the channel to protect the moving electrons in the channel from impurity scattering. The doping concentration is $2\times10^{12}\ \mathrm{cm^{-2}}$ for the upper *n*-type *δ*-doped layer and $3\times10^{12}\ \mathrm{cm^{-2}}$ for the lower one. These two *n*-type *δ*-doped layers supply electrons to the channel. The *n*-type GaAs cap layer, which has a doping concentration of $5\times10^{18}\ \mathrm{cm^{-3}}$, is used to form the ohmic contact.

The barrier in the typical HEMT (Fig. 1a) consists of a single 100-Å-thick intrinsic InGaP layer. On the other hand, the barrier in the HEMT shown in Fig. 1b consists of a 100-Å-thick intrinsic InGaP layer in which a *p*-type *δ* doping is located 80 Å above the bottom edge. Three different *p*-type *δ*-doping concentrations are investigated in our simulation: $1\times10^{12}\ \mathrm{cm^{-2}}$, $2\times10^{12}\ \mathrm{cm^{-2}}$, and $3\times10^{12}\ \mathrm{cm^{-2}}$. The metal/InGaP Schottky potential energy is set to 0.9 eV according to the published experimental results [10, 11]. The gate length in both devices is 0.5 μm; the source–drain distance and the recess width (cap to cap) are 3 μm and 1 μm,

✉ Fax: +886-4/721-1153, E-mail: ykuo@cc.ncue.edu.tw

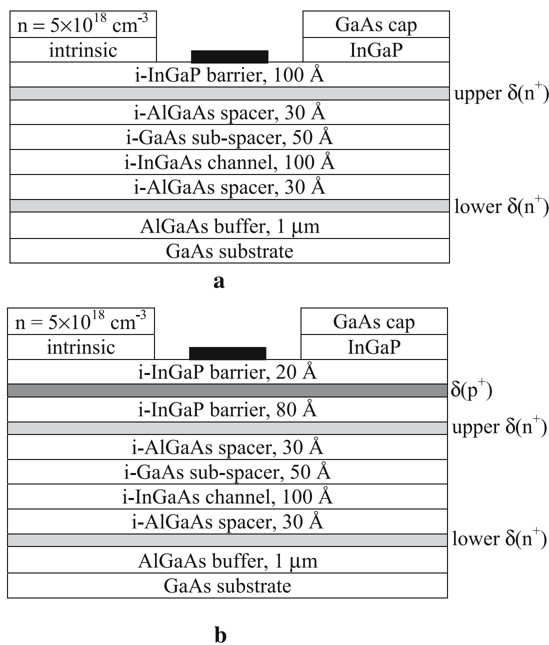

FIGURE 1 Structures for **a** a typical InGaP/InGaAs/GaAs pseudomorphic HEMT and **b** a HEMT with a p-type δ-doped InGaP barrier

respectively. For a two-dimensional simulation, we exclude the influence of gate width.

3 Simulation results and discussion

Figure 2 shows the energy-band diagram and the distribution of electron concentration for the HEMT with a p-type δ-doped InGaP barrier that has a doping concentration of 3×10^{12} cm^{-2}. The biases of source, gate, and drain are all set to 0 V. As shown in Fig. 2, the electrons tend to accumulate in the lower edge of the channel layer. The highest electron concentration in the channel is about 2.5×10^{19} cm^{-3}. It is obvious that the p-type δ-doped region is fully depleted. The depletion is very crucial and should be maintained even under biased conditions to prevent conduction between gate and source, and gate and drain [7]. When applying a positive bias to the gate terminal, we find that the barrier height increases with the applied gate bias. One may expect that the larger barrier height should contribute to the decrease of electron tunneling from the channel to the gate while the device is operating in the on state.

Figure 3 shows the dc I–V characteristics of the typical HEMT and the HEMT with a p-type δ-doped InGaP barrier that has a doping concentration of 3×10^{12} cm^{-2}. The source and drain terminals are both grounded. The gate tunneling effect and the impact ionization effect have been taken into account in this simulation. If we define the voltages at which the leakage current reaches ± 1 mA/mm as the turn-on and breakdown voltages, the turn-on voltage is 0.42 V for the typical HEMT and 1.13 V for the one of our design. The higher turn-on voltage for the HEMT with a p-type δ-doped InGaP barrier is due mainly to its larger barrier height. The breakdown voltage for the device with a p-type δ-doped InGaP barrier is 7.2 V, which is two times higher than 3.5 V for the typical HEMT. However, under a negative gate bias condition the barrier height of our device is not higher than that of the typical HEMT. The relatively high breakdown voltage originates from the electric field produced by the negative charges in the depleted p-type region. In principle, a higher barrier height would certainly be beneficial for carrier confinement, such that good linearity of device operation could be expected [5, 7, 9, 12].

The transconductances of the typical HEMT and the HEMTs with p-type δ-doped barriers of various doping concentrations are shown in Fig. 4. The drain to source voltage for the typical HEMT is set to 1.8 V and the others are set to 2.2 V, because electrons leak to the gate easily in the typical HEMT when the drain to source voltage exceeds 2.0 V. Figure 4 indicates that, for high reverse gate bias (a gate bias smaller than -0.4 V), all devices have almost equal transconductance. However, for the device with a p-type δ-doped InGaP

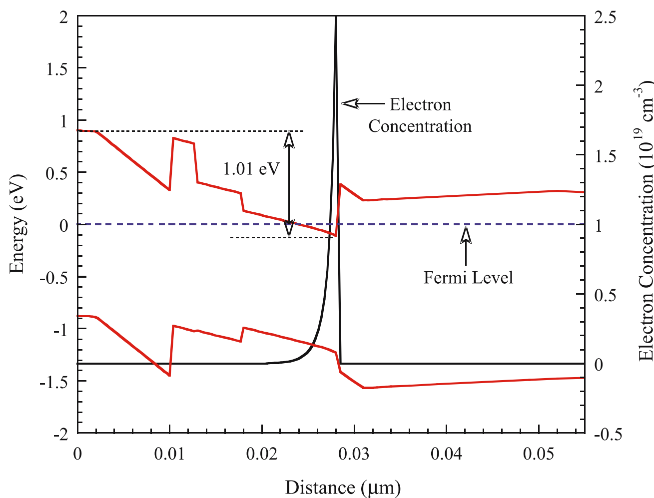

FIGURE 2 Energy-band diagram and distribution of electron concentration for the HEMT with a p-type δ-doped InGaP barrier that has a doping concentration of 3×10^{12} cm^{-2}

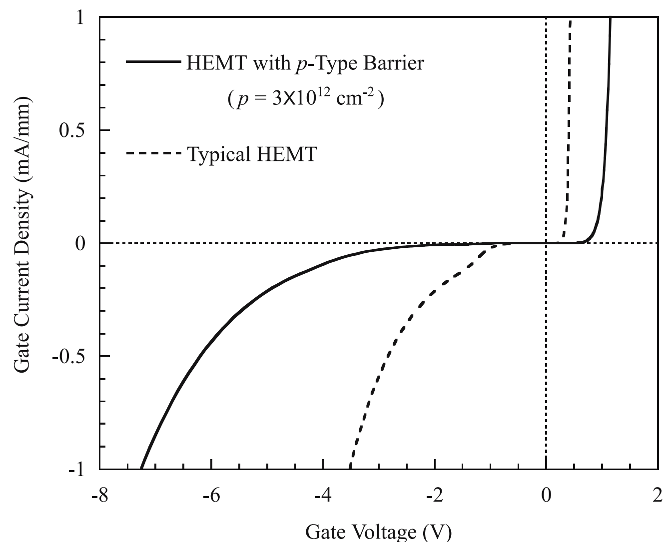

FIGURE 3 Direct-current I–V characteristics of the typical HEMT and the HEMT with a p-type δ-doped InGaP barrier that has a doping concentration of 3×10^{12} cm^{-2}

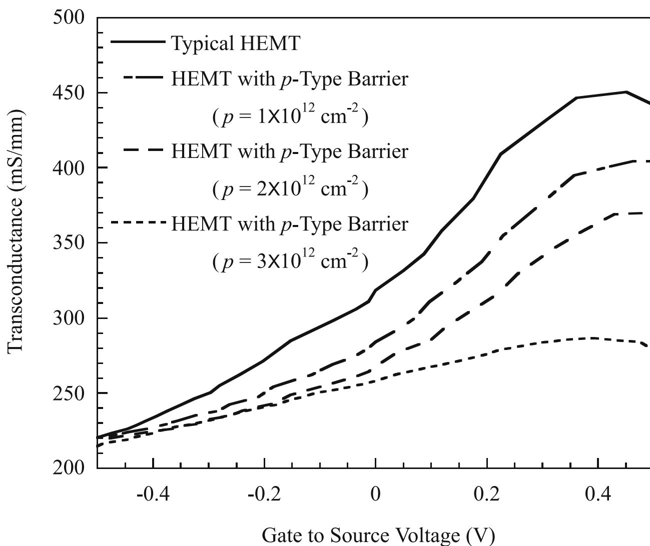

FIGURE 4 Transconductance of the typical HEMT and the HEMTs with p-type δ-doped barriers of various doping concentrations

barrier, the depletion width of the channel is less dependent on gate bias; thus a relatively voltage-independent transconductance may be obtained. This phenomenon is more evident at high p-type doping concentration [7, 12]. It is believed that the use of p-type δ doping leads to a higher barrier potential and better carrier confinement.

In addition to the smaller and relatively voltage-independent transconductance, we have also observed that the device with a p-type δ-doped InGaP barrier has a smaller gate capacitance (not shown here). This is consistent with the result reported in [12]. Moreover, for short-channel devices, the ratio of transconductance to gate capacitance, g_m/C_{gs}, depends on material parameters and geometrical factors only, not on layer structure. Therefore, the high-frequency performance of the device with a p-type δ-doped InGaP barrier should be similar to that of a typical one [12].

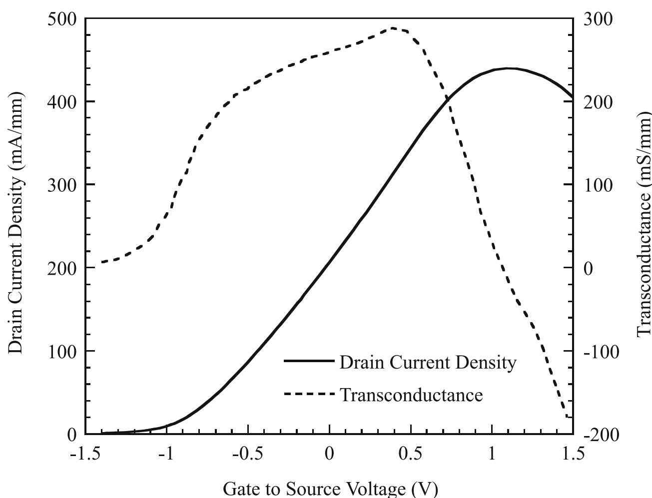

FIGURE 5 Drain-current density and transconductance as a function of gate to source voltage for the HEMT with a p-type δ-doped InGaP barrier that has a doping concentration of 3×10^{12} cm^{-2}

Figure 5 shows the drain-current density and the transconductance as a function of gate to source voltage for the HEMT with a p-type δ-doped InGaP barrier that has a doping concentration of 3×10^{12} cm^{-2}. The drain voltage is 2.2 V, which is identical to that used in Fig. 4. When the gate bias reaches -1.3 V, the device would be pinched off. The transconductance has a maximum value of 282 mS/mm for this device. The swing range in which the transconductance exceeds 80% of the maximum is about 1.2 V (from -0.5 V to 0.7 V). This swing range is two times larger than 0.56 V for the typical HEMT. After the gate voltage goes beyond 1.0 V, the drain current no longer increases with gate voltage; instead, it decreases with gate voltage. This is caused by the real-space transfer (RST) of hot electrons at high gate voltage. As a consequence, negative differential resistance (NDR) and negative transconductance are observed [13].

4 Conclusion

We have numerically investigated the dc characteristics of an InGaP/InGaAs/GaAs pseudomorphic HEMT with a p-type δ-doped InGaP barrier by using the ISE-TCAD simulation program. Attributed to the employment of a p-type δ-doped InGaP barrier, a higher barrier potential is obtained. The simulation results suggest that, when compared with the typical HEMT, the HEMT with a p-type δ-doped InGaP barrier has a higher gate turn-on voltage, better carrier confinement, and a relatively broader gate swing range. Furthermore, for the HEMT with a p-type δ-doped InGaP barrier, the electric field caused by the negative charges in the depleted p-type region helps to improve the breakdown voltage. These results are promising for linear and large-signal application of the HEMTs with this structure. The HEMT design suggested in this paper may be of great interest for the device-physics community.

ACKNOWLEDGEMENTS One of the authors, Y.-K. Kuo, would like to acknowledge the National Science Council of the Republic of China, Taiwan, for financial support under Grant No. NSC-92-2112-M-018-008.

REFERENCES

1 Y.W. Chen, W.C. Shu, S.M. Shieh, Y.J. Chen, Y.S. Lin, Y.J. Li, T.B. Wang: IEEE Trans. Electron Devices **49**, 221 (2002)
2 S.F. Yoon, B.P. Gay, H.Q. Zheng, H.T. Kam, J. Degenhardt: IEEE Trans. Electron Devices **47**, 1115 (2000)
3 Y.S. Lin, S.S. Lu, P.Z. Chang: J. Appl. Phys. **85**, 2197 (1999)
4 D. Geiger, E. Mittermeier, J. Dickmann, C. Geng, R. Winterhof, F. Scholz, E. Kohn: IEEE Electron Dev. Lett. **16**, 259 (1995)
5 J.H. Tsai: Electron Dev. Lett. **24**, 1 (2003)
6 W.C. Liu, K.H. Yu, K.W. Lin, J.H. Tsai, C.Z. Wu, K.P. Lin, C.H. Yen: IEEE Trans. Electron Devices **48**, 1552 (2001)
7 W.S. Lour, J.H. Tsai, L.W. Laih, W.C. Liu: IEEE Trans. Electron Devices **43**, 871 (1996)
8 W.S. Lour, W.L. Chang, S.T. Young, W.C. Liu: Electron. Lett. **34**, 814 (1998)
9 M. Nakamura, S. Wada, H. Kawasaki, M. Abe, I. Hase: Electron. Lett. **35**, 336 (1999)
10 L.P. Sadwick, C.W. Kim, K.L. Tan, D.C. Streit: IEEE Electron Dev. Lett. **12**, 626 (1991)
11 S.C. Yang, H.C. Chiu, Y.J. Chan, H.H. Lin, J.M. Kou: IEEE Trans. Electron Devices **48**, 2906 (2001)
12 S. Sassen, B. Witzigmann, C. Wolk, H. Brugger: IEEE Trans. Electron Devices **47**, 24 (2000)
13 R.E. Thorne, S.L. Su, R.J. Fischer, W.F. Kopp, W.G. Lyons, P.A. Miller, H. Morkoc: IEEE Trans. Electron Devices **30**, 212 (1983)